

## Review

# Recent Advances in Nanowire-Biosystem Interfaces: From Chemical Conversion, Energy Production to Electrophysiology

Lin Xu,<sup>1,3</sup> Yunlong Zhao,<sup>2,3</sup> Kwadwo Asare Owusu,<sup>1</sup> Zechao Zhuang,<sup>1</sup> Qin Liu,<sup>1</sup> Zhaoyang Wang,<sup>1</sup> Zhaohuai Li,<sup>1</sup> and Liqiang Mai<sup>1,\*</sup>

The nano-bio interface generated by integrating semiconductor nanomaterials with living cells could serve as a platform for facilitating energy and signal transfer between non-living materials and living systems for applications in energy and the life sciences. This review presents recent advances in one-dimensional nanomaterial-biosystem interfaces and applications from chemical conversion and energy production to electrophysiology. First, we introduce representative types of nanowire-biosystem interfaces and their design principles. Second, we present nanomaterial-bacteria hybrids for solar-to-chemical CO<sub>2</sub> reduction. Third, we introduce nano-bio hybrid electrodes for energy production, especially for biofuel cells. Fourth, we present semiconductor nanowire-embedded nanoelectronics interfaced with living cells and tissue for electrophysiological signal recordings. Last, we provide a brief summary of the progress on energy and signal transfer at the nano-bio interface, as well as our perspectives on the challenges and future directions in this interesting field.

## INTRODUCTION

Human civilization relies heavily on the development of both sustainable energy and biology and medicine. Although inorganic materials or living organisms can be used independently in the field of energy and biology, inorganic-biological hybrid systems could combine the strengths of both non-living materials and living organisms. Moreover, because many chemical reactions and biological functions occur at nanoscale, studying the nanowire-biosystem interface is particularly useful for understanding the underlying chemical and physiological processes, and could open up new vistas for more efficient energy production and conversion, physiological diagnostics, and therapeutics. Here, three representative fields, namely solar-to-chemical CO<sub>2</sub> reduction, biofuel-to-electricity-induced energy production, and electrophysiology, are introduced to stimulate the design of nanoscale inorganic-biological hybrid systems. In the field of photosynthetic CO<sub>2</sub> reduction, a limited number of enzymes isolated from biological system can absorb light and catalyze CO<sub>2</sub> into a single chemical product with high selectivity and low energy barriers, but this process is only 0.5%–2.0% efficient. The efficiency of nanoscale inorganic semiconductor photovoltaics can reach up to ~20%, but the selectivity and purity of the chemical products from CO<sub>2</sub> reduction is low.<sup>1</sup> Thus, a nanoscale inorganic-biological hybrid system that combines the high solar-to-energy efficiency of inorganic semiconductor material as a broadband light harvester and the high-selectivity chemical production ability of living organisms would be promising for artificial photosynthetic CO<sub>2</sub> reduction. In the field of biofuel-to-electricity-induced energy production, electricity-generating bacteria can oxidize organic

## The Bigger Picture

Interfacing nanoscale semiconductor and biological systems is an emerging interdisciplinary field of science and technology bridging chemistry, biology, physics, and many areas of energy, environment, and medicine. For example, combining the strengths of high solar-to-energy efficiency semiconductor materials and living organisms capable of metabolic fuel production would be promising for artificial photosynthetic CO<sub>2</sub> reduction. Merging nanowire-embedded nanoelectronics with living cells and tissue would open up the field of nano-bioelectronics to map the signals and activity in the brain with high spatiotemporal resolution. In this review, we summarize recent advances in nanowire-biosystem interfaces and applications from chemical conversion and energy production to electrophysiology and future prospects in the areas of nano-bioenergy and nano-bioelectronics.



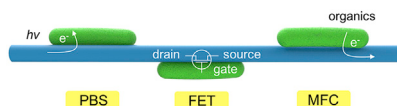


**Figure 1. Overview of Nanowire-Biosystem Interfaces**

This schematic combines the applications of nanowire-biosystem interfaces in three major fields: (1) artificial photosynthetic biohybrid system (PBS) for chemical conversion, (2) microbial fuel cell (MFC) for energy production, and (3) nanoscale field-effect transistor (FET) for high-resolution electrophysiological signal recordings. Nanowires are blue and cells are green in the schematic.

matter and produce current, which is environmentally benign but has low power density and efficiency. To address this issue, incorporating conductive one-dimensional (1D) nanowire (NW) or nanotube networks with bacteria could greatly enhance electron transfer from the bacteria to inorganic electrodes, which significantly improves the electrochemical performance, including the capacity, rate performance, cycling stability, and so on. In the field of electrophysiology, electrocardiography and electroencephalography are widely used for heart and brain examinations and diagnosis. However, realizing high spatial and temporal resolution in cellular recordings simultaneously is not feasible with these techniques. One of the smallest inorganic signal-processing units, the NW-based field-effect transistor (FET), has the potential to allow extra- and intracellular recordings with high spatiotemporal resolution.

In this review, we focus on the NW-biosystem interface as a platform where energy and signal are transferred between inorganic nanomaterials and living organisms (Figure 1). Regarding energy transfer, in a photosynthetic biohybrid system (PBS), solar energy is absorbed by semiconductor nanomaterials and the electrons generated are transferred to catalytic bacteria for artificial photosynthesis; in reverse, the electrical energy generated by chemical-consuming-bacteria can be transferred to inorganic nanostructured electrodes as microbial biofuel cells (MFCs). Regarding signal transfer, electrical signals propagated between cells and tissue in living organisms can be captured and then coupled to nanomaterial-embedded electronic devices via a nanoscale FET, which is crucial for fundamental biophysical research as well as medical monitoring and intervention. We summarize the recent progress in energy and signal transfer at the NW-biosystem interface, especially the 1D nanostructure-biosystem interface, and provide some understanding on combining the strengths of both non-living materials and living organisms. Because of the similar characteristics of various 1D nanostructures with different aspect ratios and inner structures, such as NWs, nanofibers, nanoribbons, nanobelts, nanorods, and nanotubes, they have been classified as NWs in this review for simplicity.

The construction of an NW-biosystem interface requires (1) synthesis of diverse NW building blocks, (2) culture or dissection of living cells or tissues, and (3) final integration of functional NW-biological systems. In the next section, we first emphasize the design principles of NW-biosystem interfaces and introduce representative cases based on basic and complex NWs. Then, we review the integration of nano-bio systems for detailed applications in the following sections.

## TOPOLOGICALLY DESIGNED NANOWIRES FOR NANOWIRE-BIOSYSTEM INTERFACES

The interface between a NW and a biosystem is a significant issue across broad areas of science and technology and attracts many researchers and ideas from materials

<sup>1</sup>State Key Laboratory of Advanced Technology for Materials Synthesis and Processing, International School of Materials Science and Engineering, Wuhan University of Technology, Luoshi Road 122, Wuhan 430070, P.R. China

<sup>2</sup>Department of Chemistry and Chemical Biology, Harvard University, Cambridge, MA 02138, USA

<sup>3</sup>These authors contributed equally

\*Correspondence: mlq518@whut.edu.cn

<https://doi.org/10.1016/j.chempr.2018.04.004>

science, biology, chemistry, energy, and electronics. Many efforts have been devoted to this issue in this decade, and various NW topology optimization tactics for NW-biosystem interfaces have been developed, including surface modification, morphology control, and array design. These tactics include, but are not limited to, enhancement of selective capture ability of biological targets, biosystem adhesion and/or seal resistance of NW-biosystems, to improve the performance and practicality of the hybrid system. In this section, we begin with basic NWs with obvious superiority for various biological applications over bulk materials, followed by a summary of diverse complex NWs with improved hybrid system properties or special functions for biological applications.

### Basic Nanowires for Nanowire-Biosystem Interfaces

NWs exhibit obvious superiority for various biological applications over bulk materials because of their nanoscale size and morphology tunability. The small size, high specific surface area, and 1D structure of NWs often lead to close contact with biosystems and long-range signal transfer. NWs can be mainly discussed on the basis of the following four aspects: thickness, length, shape, and arrangement. In general, various NWs can be synthesized via bottom-up or top-down approaches.<sup>2–4</sup> The bottom-up strategy focuses on building or assembling NWs from atomic or molecular components, such as gas-phase growth and solution-phase routes. The top-down approach seeks to fabricate NWs directly by using increasingly high-resolution lithography, etching, depositing, and 3D printing. Requirements for NW morphology and arrangement vary dramatically for different applications. For small-size biosystems, the characteristics of an ideal NW-based device should include (1) comparable thickness and length for accessible contact with biosystems and compatible interface formation, (2) high signal fidelity and sensitivity, and (3) the capability to realize multiscale signal capturing at either single biosystem or mass level. Size-tunable basic NWs with straight and homogeneous shape are suitable for efficient small-size biosystem adhesion or behavior recording.

By recording the contacts at NW-biosystem interfaces, basic NWs and their arrays can be utilized to reveal the biosystem evolution, behavior, and physiology at different dimensions. On the one hand, the small size of NWs can match well with micro- or nanoscale cells to achieve recording of biosystem behavior. Jeong et al.<sup>5</sup> presented direct evidence that *Shewanella oneidensis* MR-1 can recognize nanoscale structures by utilizing a well-defined silicon NW array platform and single-cell imaging (Figure 2A). Accordingly, bacterial swimming patterns and initial attachment locations are strongly affected by the presence of NWs on a surface. Further analysis of bacterial trajectories indicated that nanoscale topography can influence bacterial movement and attachment behavior and play a significant role in the biofilm formation. They also found that, compared with a single NW, a NW array better recorded the interactions of NW/bacteria at the single-cell level. The surface of NWs can be further functionalized in simple forms by different chemicals. These results demonstrate the immense significance of basic NW-bio interfaces, and that homogeneous NWs and their arrays are appropriate for small-size biosystems. On the other hand, NWs with high specific surface area also possess wide potential. Abundant surface sites of NWs can gather and record more data and signals. Cui et al.<sup>6</sup> reported a series of surface-functionalized NWs as highly sensitive, real-time electrically based sensors for many biological and chemical species. They found that the small size and capability of these NWs can greatly increase recording sensitivity and achieve array-based screening and *in vivo* diagnostics. Patolsky et al.<sup>7</sup> also reported NW-based FETs with high selectivity for direct and real-time electrical detection of single virus particles (Figure 2B). The multiple surface sites of NW arrays

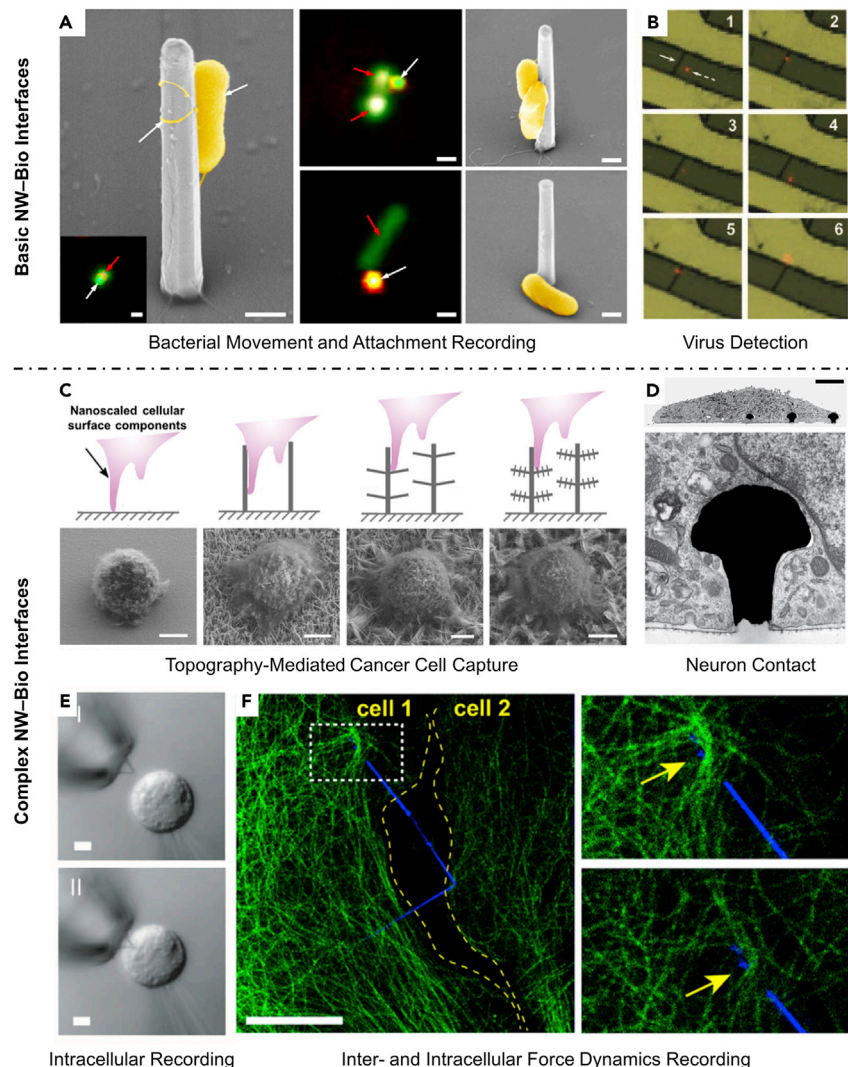


**Figure 2. Typical Examples of Nanowire-Biosystem Interfaces**

(A) SEM and fluorescence images of MR-1 cells on Si nanowires. MR-1 cells were preferentially adhered on the Si nanowires with alignment along the nanowire lengthwise direction. Some MR-1 cells were also observed on the bottom substrate but still in close contact with the nanowires. Red and white arrows indicate MR-1 cells and Si nanowires, respectively. Reprinted with permission from Jeong et al.<sup>5</sup> Copyright 2013 American Chemical Society.

(B) Combined bright-field and fluorescence images; a virus appears as a red dot in the images. Images 1–6, recorded over different time periods, indicate a single virus binding to and unbinding from the nanowire. Solid and dashed white arrows indicate the positions of the nanowire device and a single virus, respectively. The size of each picture in (B) is  $8 \times 8 \mu\text{m}$ . Reprinted from Patolsky et al.<sup>7</sup> Copyright 2004 National Academy of Sciences.

(C) Typical morphologies of captured MCF7 cells on different biointerfaces. Reprinted with permission from Zhang et al.<sup>9</sup> Copyright 2016 American Chemical Society.

(D) Electron micrograph of a mushroom nanowire engulfed by a PC12 cell. The black spine indicates gold mushroom nanowires. Reprinted by permission from Springer Customer Service Centre GmbH: Springer Nature, *Nature Methods*, Hai et al.,<sup>10</sup> copyright 2010.

(E) Differential interference contrast microscopy images of an HL-1 cell interfaced with a kinked nanowire probe as the cell approaches (I) and contacts and internalizes (II). Reprinted with permission from Tian et al.<sup>11</sup> Copyright 2010 AAAS.

(F) Micrograph of time-lapse live-cell confocal fluorescence shows HASMC (human aortic smooth muscle cell) microtubule bundles (green) interacting with a kinked Si NW (blue) at  $T = 0 \text{ min}$  (left and

**Figure 2. Continued**

upper right) and T = 24 min (lower right). Yellow arrows indicate that the KSiNWs were pinned intercellularly in the cytoskeleton network. Reprinted with permission from Zimmerman et al.<sup>12</sup>

Copyright 2015 American Chemical Society.

Scale bars represent 500 nm (A), 5 μm (C), 5 μm (D, top), 500 nm (D, bottom), 5 μm (E), and 10 μm (F).

modified with antibodies specific for viruses enable rapid identification. NWs offer new and sometimes unique opportunities to fabricate novel biosensors.<sup>8</sup> NWs represent outstanding primary transducers for recording signals that eventually interface to macroscopic instruments. Over the decade, the design of NW-biosystem interfaces with straight and homogeneous basic NWs has led to many advances that may allow for direct, fast, accurate, and multiscale analysis of biological species and cellular activities. But, further development of these basic NW-biosystem devices beyond the prototype stage lie not only in delicate NW-based device integration but also in detailed insights into the biochemical mechanisms between NWs and biosystems.

### Complex Nanowires for Nanowire-Biosystem Interfaces

Basic NWs and their devices need to be structurally modified for stronger biosystem adhesion and seal resistance, leading to a more compatible NW-biosystem interface. Utilization of complex NWs with specific morphology and multiple sites holds the key to unlocking the potential of NW-based devices. Toward improving cell adhesion, Kong et al.<sup>13</sup> demonstrated a bio-inspired antenna-like nanocube-terminated NW array as a unique platform that can recognize 3D signal molecules and can be used for biosensing. Living-cell adhesion and *in situ* cultivation on this NW array, which integrates with sensitive electrochemical recording of cellular activity in real time, are realized by rational incorporation between Prussian blue nanocube heads and TiO<sub>2</sub> NW arms. Optimization of NW topology for more efficient biosystem capture has also attracted interest. Zhang et al.<sup>9</sup> fabricated a hierarchical assembled indium-tin-oxide NW array with both horizontal and vertical NW branches for the capture of cancer cells (Figure 2C). The introduction of horizontal and vertical nanowire branches greatly enhances the topographical interactions between cancer cells and branchy NWs, which match better with cell filopodia and provide more binding sites than basic NWs. This work opens up a new avenue for rational design of NW-biosystem interfaces for advanced biological applications. Increasing the sealing resistance to enhance the intensity of signals is another goal for NW topology optimization. Hai et al.<sup>10</sup> reported a method of “intracellular recording” that induces positive engulfment of *Aplysia californica* neurons in prominent microelectrodes, providing subthreshold synapses and action potentials that match the signal-to-noise ratio of traditional intracellular recordings. They cultured a neuron on a micrometer-size mushroom-shaped spine-like NW array (Figure 2D). The unique NW shape promotes tight connection with the cell membrane, increases the sealing resistance, and enhances the electrical coupling between the cells and the functionalized gold-spine electrodes. The implementation of this approach may open up new prospects for neuroscience and biomedical applications.

Complex NWs also realize other functions. For intracellular recording, Tian et al.<sup>11</sup> designed a unique kinked nanowire (KNW) probe by surface modification with unilamellar vesicles of phospholipid bilayers (Figure 2E). They monitored the potential change in a phospholipid-modified KNW-based probe when an isolated HL-1 cell was moved into contact and then away from the KNW with a glass micropipette. A sharp potential drop was recorded after cell-to-tip contact, and the potential returned to the original level when the cell was detached from the probe end. For

another probe without surface modification, no additional potential changes were observed as the HL-1 cell was brought into contact and then retracted. Furthermore, Xu et al.<sup>14</sup> designed and fabricated three types of functional KNWs, including U-shaped structures, V-shaped structures, and W-shaped multiplexed KNWs. In their work, the angle and number of kinks can be tuned during NW growth. The U-shaped 3D KNWs reduce the entire probe cross-sectional area and provide a better choice for applications that require deep insertion into cells. More interestingly, cellular force monitoring can be realized on KNWs. Zimmerman et al.<sup>12</sup> showed that label-free KNWs as inter- and intracellular force probes can be internalized in multiple cell lines, forming robust cytoskeletal interfaces (Figure 2F). These significant results indicate that the shapes and surfaces of NWs featuring high biocompatibility hold great significance for assisting entry to intracellular regions through cell membrane fusion. The facile design and bottom-up synthesis of these KNWs and devices greatly promote the development of life science.

In summary, the dimension, geometry, and composition of NWs can be tuned in high resolution for different biological applications.<sup>2–4</sup> The above-mentioned basic and geometry-modulated NWs can serve as diverse functional nanoscale building blocks for interfacing with biological systems for various applications as reviewed in the following sections.

### NANOMATERIAL-BACTERIA HYBRIDS FOR CHEMICAL CONVERSION

Compared with chemical catalysts, photosynthetic organisms present near 100% selectivity for CO<sub>2</sub> reduction into useful fuels; however, the solar-to-energy efficiency of this process is extremely low.<sup>1</sup> On the other hand, solar energy conversion efficiency approaching 20% has been realized in inorganic semiconductor light harvesters. Despite this achievement, the abiotic electrochemical reduction of carbon dioxide is hindered by high cost, poor stability of cathodes, a sluggish CO<sub>2</sub> reduction process, and non-specificity of the products produced. A hybrid system that integrates highly selective biological catalysts and high-efficiency light harvesters would be viable for reducing CO<sub>2</sub> with efficiencies exceeding either biotic or abiotic CO<sub>2</sub> reduction.<sup>15</sup> Recent studies have focused on designing biocompatible nanomaterial-bacteria hybrids referred to as PBSs for chemical conversion. Gram-negative facultative bacteria including *Shewanella oneidensis* MR-1 and acetogenic *Sporomusa ovata* have been well documented for easy formation of biofilms and microbial electrosynthesis.<sup>16,17</sup> For instance, *S. oneidensis* MR-1 undergoes indirect extracellular electron transfer by using electron shuttles to produce electricity with lactate as an electron donor, whereas *S. ovata* accepts electrons from graphite electrodes to reduce CO<sub>2</sub> into acetate and other useful fuels.

Nanostructured materials, especially NWs, are promising for nanomaterial-bacteria hybrid systems because of their desirable properties, such as large surface area, mechanical flexibility, comparable nanoscale dimensions with bacteria cells, and interfacial biocompatibility. Importantly, NWs could provide an avenue for studying the interactions between nanomaterials and bacteria in hybrid systems. For example, utilizing real-time optical imaging and mathematical modeling techniques, Yang and co-workers successfully showed that *S. oneidensis* MR-1 bacteria exhibit preferential attachment and perfect alignment to Si NW arrays.<sup>5</sup> In a subsequent work, Yang and co-workers further demonstrated that the orientation of bacteria attachment to NW arrays is affected by several factors, including temperature, pH, pressure, etc., and that the growth of *S. ovata* cells on vertical Si NW arrays can be controlled by simple changes in ionic concentrations.<sup>18</sup> PBSs can be divided into

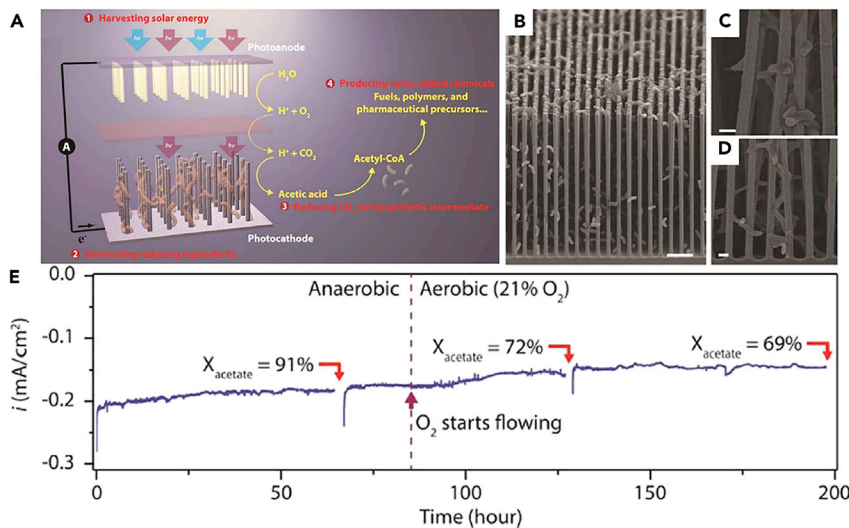


**Figure 3. Integrated Silicon Nanowire-Bacteria PBS for CO<sub>2</sub> Reduction**

(A) Schematic of the Si-Sporomusa ovata biohybrid system for the production of acetate and other useful fuels.  
 (B) Cross-sectional SEM image of the three-dimensional network in the nanowire-bacteria hybrid.  
 (C and D) Magnified images of the middle (C) and bottom (D) regions of the nanowire array in the vertical direction.  
 (E) Aerobic CO<sub>2</sub> reduction by *S. ovata* upon loading Pt onto the nanowire electrode.

Reprinted with permission from Liu et al.<sup>20</sup> Copyright 2015 American Chemical Society. Scale bars represent 5 μm (B) and 1 μm (C and D).

two categories: integrated PBSs and distributed PBSs. In integrated PBSs, the bacteria are directly in contact with the inorganic light harvester and hence, the mechanism of electron transfer involves a one-step transfer of e<sup>-</sup> from the light harvester to the biological component for CO<sub>2</sub> reduction. On the other hand, distributed PBSs are characterized by discrete steps where molecular reducing equivalents first produced via light harvesting are used to reduce CO<sub>2</sub> to derive useful fuels such as methane.<sup>19</sup> This section of the review covers some of the major advances in the field of PBSs via these two approaches as well as the possible electron-transfer process.

### Integrated Photosynthetic Biohybrid Systems

Biocatalysts allow the reduction of CO<sub>2</sub> into biosynthetic intermediates, which act as building blocks for producing fuel; however, these bacteria do not function properly when exposed to oxygen and hence cannot be utilized to reduce CO<sub>2</sub> sources containing oxygen. To circumvent this problem, Yang and co-workers developed a biocompatible nanomaterial-bacteria hybrid by interfacing Si NW arrays with *S. ovata* bacteria for the reduction of CO<sub>2</sub> under mild conditions (Figure 3A).<sup>20</sup> The Si NWs synthesized through reactive-ion etching of single crystalline Si wafers perform several functions for the successful reduction of CO<sub>2</sub> to produce acetate under aerobic conditions. First, they serve as a light harvester and generate reducing equivalents for CO<sub>2</sub> reduction. Second, the NW morphology not only provides a large surface area for interfacing the *S. ovata* microbes, it also creates an anaerobic environment that is beneficial for CO<sub>2</sub> reduction under aerobic conditions. The cross-sectional scanning electron microscopy (SEM) images of the biohybrid system displayed in Figure 3B show that the *S. ovata* bacteria and the Si NWs are interconnected in a 3D network. Importantly, higher-magnification SEM images (Figures 3C and 3D) show that the bacteria are uniformly deposited on the Si NWs without impeding pathways for mass transport. The NW-bacteria biohybrid system is

characterized by a low overpotential, a high faradic efficiency of 90%, and long-term stability up to 200 hr. One major advantage of the biohybrid system is that it allows CO<sub>2</sub> reduction to produce acetate in aerobic conditions. The production of acetate with *S. ovata* bacteria occurs through the Wood-Ljungdahl pathway. Specifically, acetic acid is produced with a faradic efficiency of 70% when the NW arrays are loaded with Pt catalysts (Figure 3E). Remarkably, the acetate produced can be activated in the presence of *Escherichia coli* to obtain the biosynthetic intermediate acetyl-CoA, which serves as a building block for the biosynthesis of complex molecules. This biohybrid system differs from conventional microbial electrosynthesis because it permits interactions between the bacteria and light harvesters in a single solid-state device. The efficiency of an integrated Si NW-based system for direct solar water splitting can further be augmented by utilizing two light-absorbing materials in a “Z-scheme” system. Using two light-absorbing materials, such as Si and TiO<sub>2</sub> as the photocathode and photoanode, respectively, would allow the capture of photons with lower energy and the separate generation of O<sub>2</sub> and H<sub>2</sub>, respectively. Attributable to a unique nanotree core-shell heterostructured morphology, an Si/TiO<sub>2</sub> photoelectrode loaded with co-catalysts mimics the photosynthetic process in chloroplasts and exhibits efficient water splitting with a high solar-to-fuel conversion efficiency of 0.12%.<sup>21</sup>

The chemical synthesis of light-absorbing semiconductors as well as their successful integration into biotic systems is impeded by several challenges such as high-purity reagents, complex microfabrication techniques, extreme synthesis temperatures, and compatibility issues with bacteria. To address these shortcomings, self-photosynthesizing non-photosynthetic microorganisms could be used to induce the precipitation of light-absorbing semiconductor nanomaterials from both photosynthetic and non-photosynthetic organisms. This route allows the formation of a biocompatible nanomaterial under mild conditions. *Moorella thermoacetica*, an acetogenic and electrotrophic bacterium allows the precipitation of CdS nanoparticles in the presence of Cd<sup>2+</sup> and cysteine (Cys) (Figure 4A).<sup>22</sup> The precipitated CdS serves as a light harvester in the biohybrid system, providing electrons for photosynthesis. As depicted in the pathway diagram for CO<sub>2</sub> reduction in the *M. thermoacetica*-CdS biohybrid system (Figure 4B), the photogenerated electron produced from the absorption of photons generates a reducing equivalent, which is utilized in the Wood-Ljungdahl pathway to produce acetate from CO<sub>2</sub> with high selectivity. By carefully removing one or two of *M. thermoacetica*, CdS, or visible sunlight in control experiments, artificial photosynthesis in the biohybrid system was confirmed and the importance of light to maintain the viability of the *M. thermoacetica*-CdS biohybrid system was demonstrated (Figure 4C). A high maximum yield (90%) of acetic acid is produced by the biohybrid system in visible light in comparison with the poor or 0% production rates in the control samples. It is generally assumed that electron transfer in nanomaterial-bacteria hybrids for chemical conversion involves hydrogenase-dependent hydrogen shuttling followed by uptake into the Wood-Ljungdahl pathway, although the exact mechanism is poorly understood.<sup>23</sup> Compared with solid electrode systems, the *M. thermoacetica*-CdS PBS, which is a translucent colloidal suspension, offers a perfect platform for studying the pathways underlying CO<sub>2</sub> reduction into acetate by using spectroscopic techniques. Utilizing transient absorption and time-resolved infrared spectroscopy, Kornienko et al.<sup>24</sup> showed that e<sup>-</sup> transfer in the *M. thermoacetica*-CdS system follows a two-pathway mechanism depending on the absence or presence of hydrogenase. The non-hydrogenase-mediated pathway, which occurs during the first 3 hr of photosynthesis, is not efficient in reducing CO<sub>2</sub> into acetate because it is characterized by slow charge-transfer kinetics resulting in the

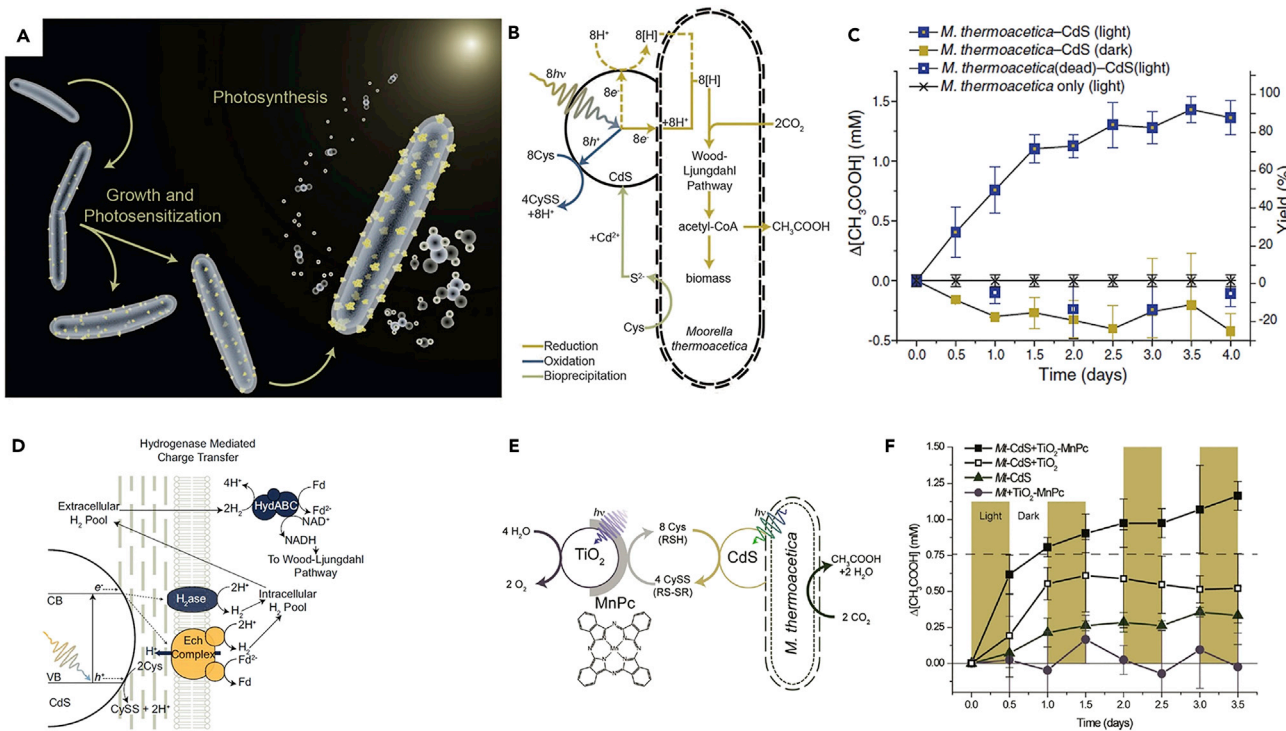


**Figure 4. Integrated CdS-Bacteria PBS for CO<sub>2</sub> Reduction**

(A–C) Schematic of the *M. thermoacetica*-CdS hybrid system showing the growth and bio-precipitation process of the CdS nanoparticles (A), pathway diagram for the *M. thermoacetica*-CdS hybrid system (B), and photosynthetic production of acetic acid by *M. thermoacetica*-CdS biohybrid systems (C). Reprinted with permission from Sakimoto et al.<sup>22</sup> Copyright 2016 AAAS.

(D) Hydrogenase-mediated pathway in the *M. thermoacetica*-CdS system. Reprinted from Kornienko et al.<sup>24</sup>

(E and F) Schematic of the *M. thermoacetica*-CdS + TiO<sub>2</sub>-MnPc tandem hybrid system (E) and comparison of acetic acid production rate of the *M. thermoacetica*-CdS and TiO<sub>2</sub>-MnPc system with control systems (F). Reprinted with permission from Sakimoto et al.<sup>25</sup> Copyright 2016 American Chemical Society.

Error bars represent the standard deviation (SD); n = 3.

recombination of holes and electrons and the non-existence of reducing equivalents such as H<sub>2</sub> and NAD(P)H. In contrast, the presence of hydrogenase drives the charge-transfer kinetics of e<sup>-</sup> to a membrane-bound hydrogenase, generating molecular H<sub>2</sub> in the process. Sufficient amounts of H<sub>2</sub> molecular equivalents accumulate in 24 hr and enter the Wood-Ljungdahl pathway by being oxidized by the HydABC complex to generate reducing equivalents for CO<sub>2</sub> reduction (Figure 4D). This work showed that the photosynthetic reduction of CO<sub>2</sub> to acetate is driven by an increasing rate of hydrogenase enzyme activity.

However, there is a drawback to the *M. thermoacetica*-CdS biohybrid system because cysteine functions as a sacrificial chemical quencher for the generated hole, resulting in the formation of the oxidized disulfide form, cystine. A modified version of the *M. thermoacetica*-CdS biohybrid system matches a TiO<sub>2</sub> light harvester loaded with MnPc co-catalysts for photooxidation and a CdS light harvester for photoreduction in a tandem Z-scheme design.<sup>25</sup> The choice of TiO<sub>2</sub> nanoparticles is crucial because they exhibit better water photooxidation ability and stability than CdS nanoparticles, and the loaded MnPc co-catalysts ensure the regeneration of the CySS/Cys redox shuttle by reducing CySS back into Cys (Figure 4E). Comparatively, the *M. thermoacetica*-CdS and TiO<sub>2</sub>-MnPc tandem system produces a higher amount of acetic acid above the stoichiometric limit of Cys

than the *M. thermoacetica*-CdS system (Figure 4F). The higher photosynthetic rate of the modified version of the biohybrid system may be attributed to the photoprotective role of TiO<sub>2</sub>.

### Distributed Photosynthetic Biohybrid Systems

Photovoltaic-driven water splitting provides a potential route for the production of hydrogen, which has potential to be a clean sustainable fuel. However, the major challenges of storage infrastructure for H<sub>2</sub> needs to be addressed before it becomes a viable option.<sup>26</sup> The advantages of photovoltaics could still be used and coupled with biohybrid systems for more efficient solar capture and CO<sub>2</sub> reduction into useful fuels and alcohols. Nocera and co-workers successfully developed a scalable bioelectrochemical system composed of cobalt phosphate (CoP<sub>i</sub>) as a water-splitting anode and nickel molybdenum zinc (NiMoZn) or stainless steel (SS) as the cathode for generating the reducing equivalents, O<sub>2</sub> and H<sub>2</sub>, respectively (Figure 5A).<sup>27</sup> The selected CoP<sub>i</sub> undergoes water splitting at low overpotentials in buffers supporting biological growth, and when coupled with the hydrogen evolution reaction (HER) catalyst, hydrogen is evolved and consumed by the bacterium, *Ralstonia eutropha* to reduce CO<sub>2</sub> into isopropanol fuel with a high yield of 216 mg L<sup>-1</sup> (Figure 5B), high selectivity, and a bioelectrochemical efficiency of 3.2% (biosynthetic leaf). The yield of isopropanol produced represents the highest values achieved for a bioelectrochemical system. However, the authors observed the generation of reactive oxygen species (ROS) arising from the oxidation of Ni with H<sub>2</sub>O<sub>2</sub> produced as by-product. This process results in the leaching of Ni, inhibiting microbial growth. To suppress the generation of ROS and solve the problem of Ni toxicity, Liu et al.<sup>28</sup> successfully addressed the incompatibility and solved the toxicity issues of the biohybrid system (Figure 5C) by replacing the NiMoZn cathode with a ROS-resistant cobalt-phosphorus (Co-P) alloy cathode. As depicted in Figure 5D, the production of H<sub>2</sub>O<sub>2</sub> is inhibited during HER, and the Co-P alloy cathode is able to maintain a stable current during a 16-day test period (Figure 5E). The Co-P and CoP<sub>i</sub> electrodes preserve the water-splitting system from Co<sup>2+</sup> leaching and, when interfaced with *R. eutropha* bacterium, a CO<sub>2</sub> reduction efficiency of ~10% for biomass, poly(3-hydroxybutyrate), and fusel alcohols such as isopropanol and isobutanol is achieved. These efficiency values far exceed the efficiency of chemical products achieved in natural photosynthetic systems.

The production of methane (CH<sub>4</sub>), a major component of natural gas via artificial photosynthesis would hold great potential, taking into consideration that the fuel could be easily fed into existing structures for delivery. However, the conversion of CO<sub>2</sub> to CH<sub>4</sub>, especially with synthetic catalysts, is a daunting task because of the large overpotentials and poor selectivity of CH<sub>4</sub>/H<sub>2</sub>. Nichols et al.<sup>19</sup> successfully developed a biohybrid system comprising earth-abundant HER  $\alpha$ -NiS electrocatalyst and *Methanobacterium barkeri*, an aerobic bacterium for CO<sub>2</sub> conversion into CH<sub>4</sub>. Evaluation of the electrocatalytic properties of the  $\alpha$ -NiS electrocatalyst shows better performances than other first-row transition HER catalysts. A high overall faradic efficiency (86%) was achieved for the reduction of CO<sub>2</sub> to CH<sub>4</sub>, coupled with a low overpotential ( $\eta = 360$  mV) as well as a high yield of 110 mL over a 7-day test period. The high yield of CH<sub>4</sub> produced along with the efficiency of the biohybrid system further corroborates the sustainability of solar-driven production of simple fuels via CO<sub>2</sub> reduction.

In summary, significant progress has been achieved in reducing CO<sub>2</sub> and water into useful chemicals by mimicking the natural photosynthetic process. Because of the

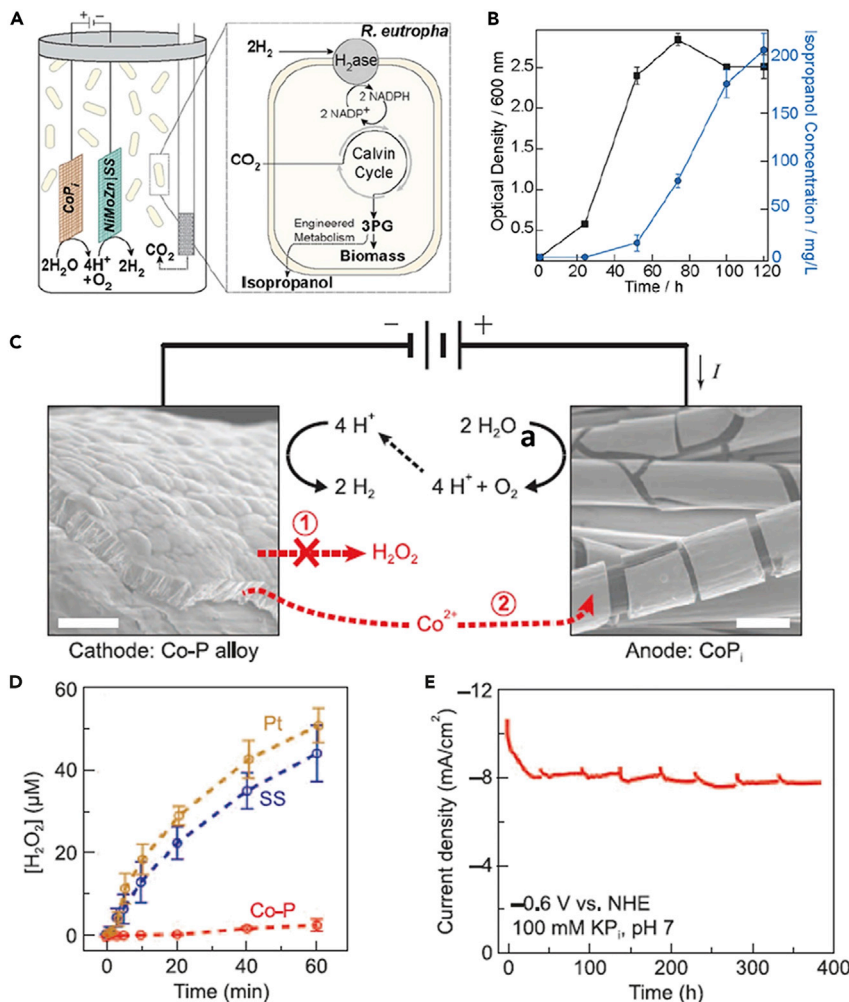


**Figure 5. Distributed PBS for  $\text{CO}_2$  Reduction**

(A) Schematic diagram of a bioelectrochemical cell for  $\text{CO}_2$  reduction to produce useful fuels by *R. eutropha* bacterium with  $\text{H}_2$  and  $\text{O}_2$  as reducing equivalents, which are generated by the  $\text{CoP}_i$  and  $\text{NiMoZn}/\text{SS}$  electrodes. Reprinted from Torella et al.<sup>27</sup>

(B) Growth and production rate of isopropanol in the  $\text{CoPi}/\text{NiMoZn}-R. eutropha$  bioelectrochemical cell. Error bars represent the standard error of the mean;  $n = 3$ . Reprinted from Torella et al.<sup>27</sup>

(C) Reaction diagram of the  $\text{Co-P}/\text{CoPi}$  biocompatible catalyst system. Scale bars represent  $10 \mu\text{m}$ . Reprinted with permission from Liu et al.<sup>28</sup> Copyright 2016 AAAS.

(D)  $\text{H}_2\text{O}_2$  accumulation for various cathodes combining with  $\text{CoPi}$  anode: yellow, Pt; blue, stainless steel (SS); red, Co-P alloy.  $E_{\text{appl}} = 2.2 \text{ V}$ . Error bars represent the standard error of the mean;  $n = 3$ . Reprinted with permission from Liu et al.<sup>28</sup> Copyright 2016 AAAS.

(E) Stability test of the Co-P alloy demonstrated by 16-day chronoamperometry. Reprinted with permission from Liu et al.<sup>28</sup> Copyright 2016 AAAS.

synergistic contributions of biological and chemical catalysts in nanomaterial-bacteria hybrids, solar energy conversion efficiencies exceeding that of natural photosynthesis have been achieved. Despite these advancements, some challenges still remain that need to be addressed to make artificial photosynthesis a definite solution to the world's energy and climate problems. Future research could be directed toward studying the viability of earth-abundant semiconductor catalysts and co-catalysts with a lower band gap to improve solar conversion efficiencies, as well as to gain an in-depth understanding of the charge-transfer mechanisms in biohybrid

devices. Finally, high-performance synthetic co-catalysts with ease of synthesis at low or moderate cost would be highly beneficial in translating biohybrid devices into practical devices.

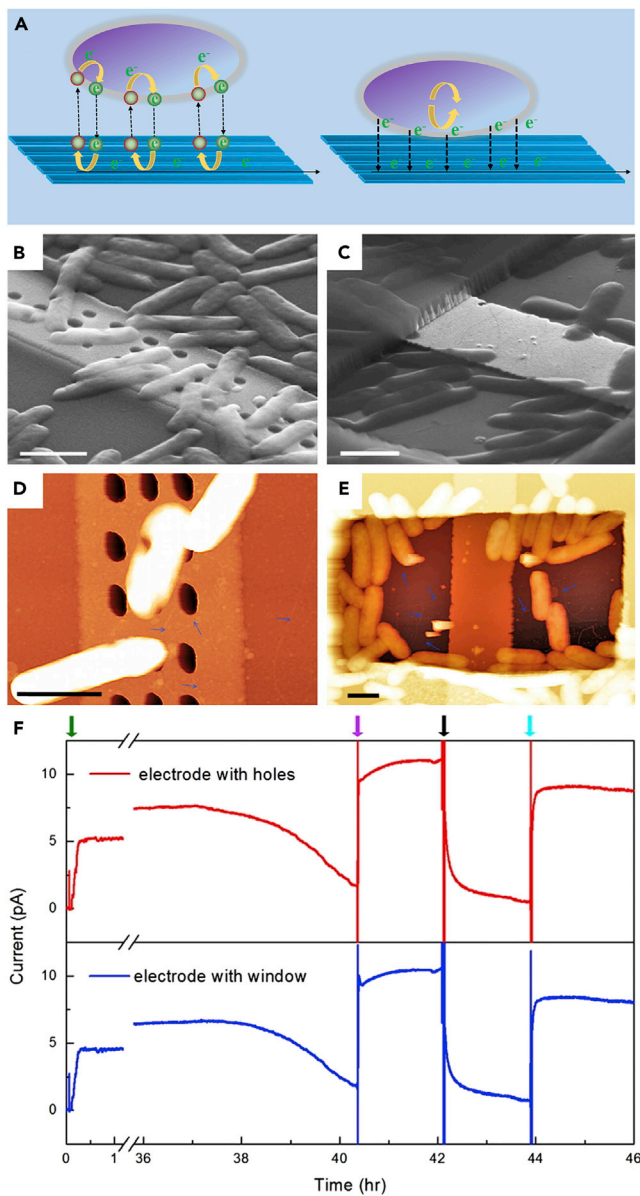
## NANOWIRE BIOHYBRID ELECTRODES FOR ENERGY PRODUCTION

Besides chemical conversion, electricity energy production is also attracting great attention because of the ever-growing demand for energy in modern society. As an example, with the aim of finding useful applications for daily waste materials and developing diverse practical energy devices, microbial technologies have been applied in energy production. In this section, we review the progress on MFCs, a well-known biological-inorganic hybrid system for energy production. MFCs are considered as an alternative power source more environment friendly than fossil fuels and have drawn intense attention from many research groups.<sup>29–32</sup> The advantages of MFCs include mild reaction conditions and the ability to produce sustainable power in a natural environment, making them easier to apply and operate than other kinds of fuel cells. In MFCs, bacteria serve as a catalyst to release electrons from organic matter (fuel source); then the electrons are transferred to inorganic conductive electrodes to generate current. Understanding how the electrons are transferred from bacteria to electrodes at the biological-inorganic interface is crucial to the further development of MFCs.

### Mechanism for Electron Transfer from Bacteria to Electrodes

In general, there are four possible kinds of mechanisms for electron transfer from bacteria to electrodes.<sup>33</sup> First, the reduced metabolic products, such as hydrogen, ammonia, or alcohols, might be oxidized at the anode surface to transfer electrons to the electrodes. Second, some artificial mediators, such as thionine, benzylviologen, phenazines, etc., serving as electron shuttles, accept electrons inside the bacteria, exit the cell in the reduced form, and then move onto the electrode surface and transfer electrons to electrodes (Figure 6A, left). Third, bacteria might produce their own mediators as electron shuttles to facilitate extracellular electron transfer. Fourth, bacteria attached on electrodes might directly transfer electrons to electrodes through the outer membrane (Figure 6A, right).

To understand which mechanism is more reasonable for a specific MFC system, it is important to design experiments to probe the interface. Jiang et al.<sup>34,35</sup> developed a general approach by using a rationally designed electrode configuration and simultaneous current recording and single-cell imaging, to identify whether the mechanism is direct electron transfer or mediated electron transfer. In their work, two kinds of electrode patterns are designed and fabricated. The conductive electrode is covered by an insulating layer with designed (1) array of nanoscale holes or (2) larger microscale exposed windows. Here, an array of nanoholes smaller in size than the bacteria precludes and a single window allows for direct microbe-electrode contacts. For the insulating layer with nanoscale holes, the cell body cannot attach the electrodes underneath, and only MFCs with a mediated electron-transfer mechanism can generate current in this case, whereas direct electron transfer is excluded. For larger microscale exposed windows, the cell body can directly attach the electrodes, and MFCs with either direct electron transfer or a mediated electron-transfer mechanism can work in this case. By combining *in situ* single-cell imaging and current recording, they can study whether there is a relationship between the number of cells attached on electrode and the current, to identify which mechanism is more reasonable. With this idea, *Shewanella oneidensis* MR-1 (MR-1) cells were studied as an example. SEM and atomic-force microscopy (AFM) images show that MR-1 cell bodies cannot attach the electrode by designed nanoholes

**Figure 6. MFC for Energy Production**

(A) Schematic of two representative electron-transfer mechanisms in the bacteria-electrode interface in MFCs. Left, mediated electron transfer; right, direct electron transfer.

(B and C) SEM images of MR-1 cells on electrodes with nanoholes (B) and window (C). Scale bars represent 1  $\mu$ m.

(D and E) AFM characterization of MR-1 cells on nanohole (D) and window (E) electrodes. Scale bars represent 1  $\mu$ m.

(F) Long-term short-circuit current measurement on electrodes with nanoholes (red) and large window (blue); the green, purple, black, and cyan arrows indicate cell addition, lactate addition, flush by fresh medium, and supernatant addition, respectively.

Reprinted from Jiang et al.<sup>34</sup>

(Figures 6B and 6D); on the other hand, MR-1 cells are in intimate contact with the exposed electrode in the large window (Figures 6C and 6E). These two cases could produce steady-state current, and the measured currents are uncorrelated with the number of cells attached on the electrodes. The short-circuit current measurements

show >70% decrease in current for both nanohole and window electrodes ranging from 38 to 40 hr (Figure 6F), which can be attributed to the depletion of electron donor (lactate) in the media. Injection of fresh medium with lactate electron donor into the chamber results in an immediate jump in current, which confirms the current is associated with bacterial metabolism. Taken together, these results indicate that electron transfer from MR-1 cell to electrode in this MFC is dominated by a mediated electron-transfer mechanism. Using the same strategy, Jiang et al.<sup>35</sup> reported the first single-cell level electrochemical studies of *Geobacter sulfurreducens* DL-1. Despite the same exposed metal area in the two types of electrodes (array of nano-scale holes versus large microscale window), current generation is only observed on the window electrode within the first 8 hr, suggesting the importance of *G. sulfurreducens* DL-1/electrode contact at the initial stage. Thus, *G. sulfurreducens* DL-1 in this MFC is associated with a direct electron-transfer mechanism.

#### Advanced Structures for MFCs

The MFC reactor consists of an anode, a cathode, and sometimes a membrane or separator between the electrodes. However, the low power density and efficiency of MFCs are major obstacles limiting their practical applications. The anode electrode material is crucial for the overall performance of MFC, and one promising route to solve this issue is to optimize the structure of the anode. Exciting progress has been made by constructing nanostructured electrodes with high surface area, especially NWs with a conductive path in the axial direction and nanosize in the radial direction, which could significantly enhance attachment and aligned growth of bacteria on NWs. Thus, NW-based electrodes show more efficiency and sustainability for MFCs than other structures such as nanospheres, nanopores, and carbon composites.<sup>36–39</sup> Cui's group described a carbon nanotube (CNT) sponge composite prepared by coating a sponge with CNTs to enhance the spatial orientation of the electrode material.<sup>37</sup> The as-fabricated electrodes have lower internal resistance, greater stability, more tunable and uniform macroporous structure (pores up to 1 mm in diameter), and improved mechanical properties and achieved a superior performance with an area power density of  $1.24 \text{ W m}^{-2}$ . They have demonstrated that these are the highest values obtained to date for MFCs fed domestic wastewater: 2.5 times the previously reported maximum areal power density and 12 times the previously reported maximum volumetric power density.

Chemical and physical modifications of anode surfaces have been used successfully to improve the performance of MFCs. Saito et al.<sup>38</sup> have discussed that the addition of nitrogen in MFC anodes could significantly increase the power densities of MFCs. Surface modifications of CNTs with metal oxides impart low contact resistance and high surface area, making them suitable for efficient electrode development. Kalathil et al.<sup>39</sup> reported a plain carbon plate (CP) modified with CNT/MnO<sub>2</sub> nanocomposite as anode for MFCs. MnO<sub>2</sub> is a transition metal oxide that has many superior electrochemical characteristics for energy storage. The Mn<sup>4+</sup> in the nanocomposite can promote electron transfer between the electrically active microorganisms and the anode material. The as-prepared anodes with high surface area result in enhanced bio-anode performance of the MFCs, which produced a maximum power density of  $120 \pm 1.7 \text{ mW m}^{-2}$ , with corresponding current density of  $0.262 \pm 0.015 \text{ A m}^{-2}$  at an external resistor of  $800 \Omega$  with an open circuit voltage of  $1.07 \pm 0.02 \text{ V}$ .

Another effective way to improve the cycling stability and power density of MFCs is to synthesize anodes with NW morphologies. It is well known that NWs have excellent electrochemical performance because of their unique characteristics and have

been widely applied for energy storage and conversion devices.<sup>40–42</sup> Zhao et al.<sup>40</sup> reported a conductive polyaniline NW network (PANI-NN) with 3D nanosized porous structures, and *Shewanella loihica* PV-4 was used as a model microbe. The microfibers were twisted and had smooth surfaces. After coating the bare graphite felt with PANI-NN, both micro- and nanosized pores were formed, indicating that PANI-NN and graphite microfibers produced hierarchical porous networks. The increased porosity and surface area led to colossal improvement in current and power densities, and an order of magnitude increase in power output was achieved. In their subsequent research,<sup>41</sup> they confirmed that the PANI-NN was able to modify the CP. Also, they found that the coating of anodes with PANI-NNs enabled substantial increases in the current and power densities (per anode geometric area) from MFCs. Analyses of the PANI-NN electrodes suggested that the large improvements were mostly ascribable to the extended surface areas of the nanostructured anodes, which could efficiently accept electrons from microbe-secreted electron mediators. Jia et al.<sup>42</sup> successfully synthesized a novel TiO<sub>2</sub> NW modified CP substrate used as bio-anode in MFCs inoculated with *Shewanella loihica* PV-4. Their work demonstrated that the surface of the carbon electrode modified with TiO<sub>2</sub> NWs can form a porous and cross-linked structure, which can greatly increase the specific surface area of the electrode and help to form a larger biofilm for improving bioelectricity generation. The TiO<sub>2</sub> NWs/CP electrode with more biofilm formed by the bacteria facilitated direct electron transfer and provided higher power density output. In conclusion, all the above results show that modification of the anodes is a favorable route to increase MFC efficiency, especially with NW modification, which provides a large number of porous structures, significantly increases the surface area, and greatly improves the electrochemical performance of the MFCs.

In summary, this versatile approach incorporating both biological and non-biological assembly strategies may provide greater flexibility for implementing advanced cell designs such as those with interdigitated microelectrodes; especially NWs will be widely exploited and used in bioenergy production systems.

## SEMICONDUCTOR NANOWIRES WITH LIVING CELLS FOR ELECTROPHYSIOLOGY

Besides the above-mentioned chemical conversion and energy production, NW-biological interfaces also play a very important role in biological or biomedical research.<sup>43–47</sup> For example, nanoscale semiconductor wire-based FETs labeled with biomarkers have been widely reported for biomolecular detection.<sup>8,48–50</sup> Non-cell-penetrating NW arrays with controllable affinity to cells have been developed for high-efficiency capture and separation of rare cells,<sup>51–53</sup> guidance of cell growth,<sup>54–56</sup> or biomechanical characterization.<sup>57,58</sup> After penetrating the cell membrane, NWs can be used for gene and biomolecular delivery with minimal invasiveness.<sup>59–62</sup> With non-penetrating or penetrating NWs, nanoelectronics have been used for optical or electrical stimulation and recording of living cells.<sup>43,63–68</sup>

Among those applications, this section of the review focuses on the interfaces between NW-based nanoelectronics and living cells for direct recording of cellular electrophysiological signals, which is important for understanding numerous physiological processes, including nerve conduction, muscle contraction, hormone secretion, etc.<sup>69–71</sup> We introduce (1) the operation schematic of a semiconductor NW-based FET, (2) extracellular electrophysiological studies of cultured cells, tissues, and organs at the *in vivo* level with the use of on-chip and/or flexible

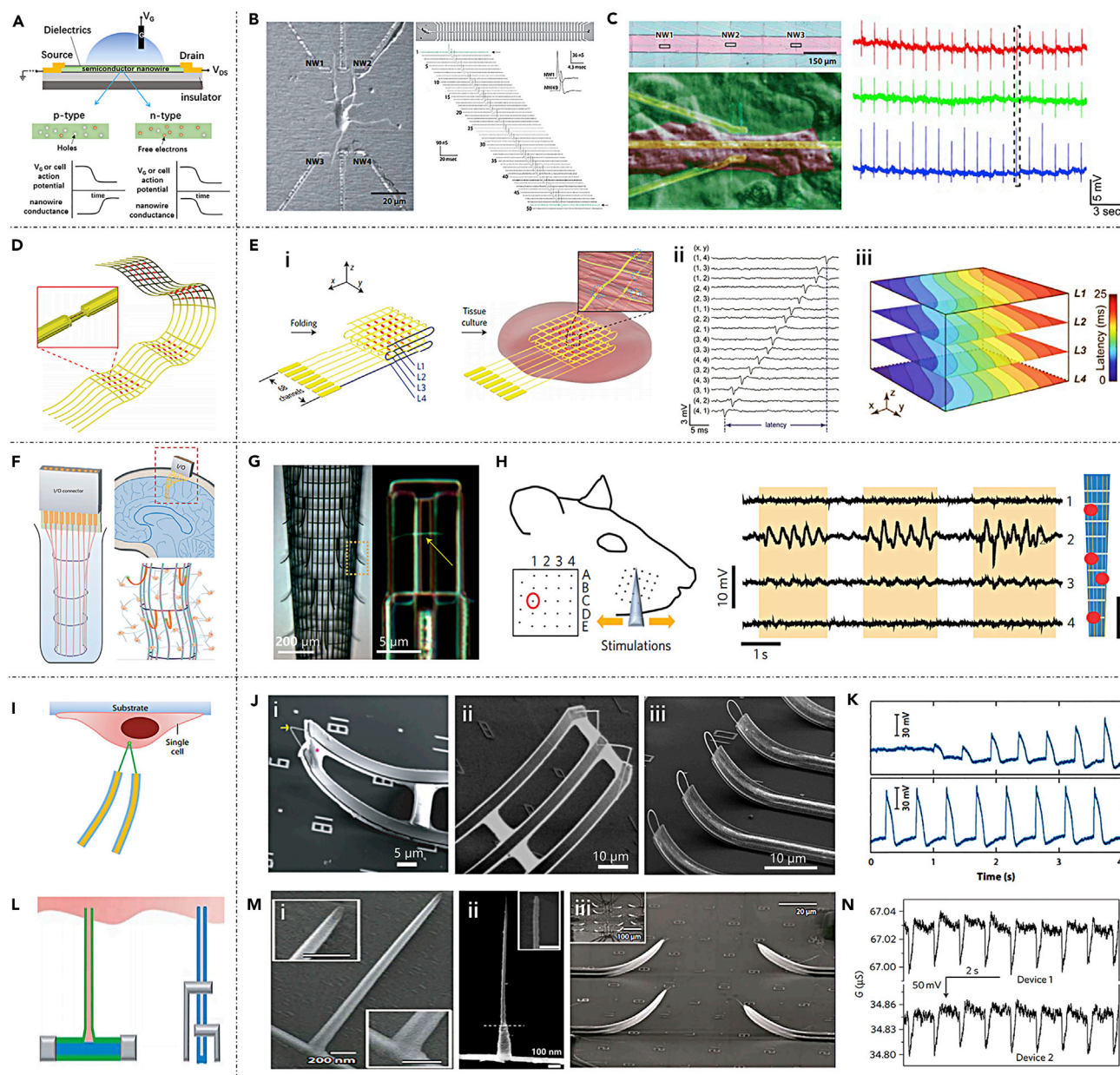


**Figure 7. Nano-FET for Electrophysiological Signal Recordings**

Extracellular electrophysiological study of cultured cells (A–C) and engineered tissues (D and E), *in vivo* extracellular electrophysiological study (F–H), and intracellular electrophysiological study by semiconductor nanowire FET (I–N).

(A) Operation schematic of a semiconductor nanowire FET.

(B) Extracellular action potential (AP) recording from cultured neurons: a cortical neuron interfaced to on-chip nanowire FETs (left), aligned axon crossing on-chip nanowire FET array (top right), and corresponding signal propagation (bottom right). Reprinted with permission from Patolsky et al.<sup>72</sup>. Copyright 2006 AAAS.

(C) Extracellular AP recording from cultured cardiomyocytes (left) and corresponding signals recorded by three on-chip nanowire FET devices (right). Reprinted from Cohen et al.<sup>73</sup>.

(D) Schematic of the free-standing macroporous nanoelectronic scaffold with nanowire FET arrays (red dots). Reprinted by permission from Springer Customer Service Centre GmbH: Springer Nature, *Nature Nanotechnology*, Dai et al.,<sup>63</sup> copyright 2016.

(E) (i) Folded 3D free-standing scaffold with FET arrays into four layers and culture of cardiac cells within the 3D folded scaffold; inset: blue circles show nanowire FETs innervate the 3D cell network. (ii) Single AP spike recorded from 16 sensors from the top layer. (iii) 3D isochronal map of time latency through the sample from all four layers. Reprinted by permission from Springer Customer Service Centre GmbH: Springer Nature, *Nature Nanotechnology*, Dai et al.,<sup>63</sup> copyright 2016.

**Figure 7. Continued**

(F–G) Schematic of the implanted macroporous nanoelectronic 3D brain probes with polymer-encapsulated metal interconnecting and supporting elements, and arms that support and connect nanowire FETs (F), micrograph of the sensor area showing the outward bent supporting arms and a typical nanowire FET voltage sensor at the end of the supporting arms (G), and acute local field potential (LFP) recording by nanowire FET sensors from the barrel cortex area (H): schematic of the correlation between the neural activity in the barrel cortex and rat whisker sensory behavior (left) and traces from four neighboring sensors (right). Reprinted with permission from Springer Customer Service Centre GmbH: Springer Nature, *Nature Materials*, Xie et al.,<sup>74</sup> copyright 2015.

(I) Schematic of intracellular electrical recordings with kinked nanowire nanoFET.

(J and K) SEM images of (i) kinked nanowire FET, (ii) W-shaped nanowire FET, and (iii) U-shaped nanowire FET arrays (J) and corresponding intracellular electrical recordings from spontaneously beating cardiomyocytes by kinked nanowire nanoFET (K). Reprinted with permission from (J, i; and K) Tian et al.<sup>11</sup> (copyright 2010 AAAS), (J, ii) Xu et al.<sup>75</sup> (copyright 2014 American Chemical Society), and (J, iii) Zhao et al.<sup>76</sup> (copyright 2016 American Chemical Society).

(L) Schematic of intracellular electrical recordings with a branched SiO<sub>2</sub> nanotube on top of a nanoFET (BIT-FET probe) and active nanotube transistor (ANTT) probe.

(M and N) SEM images of (i) standard BIT-FET probe, (ii) BIT-FET probe with sub-10-nm-diameter SiO<sub>2</sub> nanotube, and (iii) ANTT probe (M) and simultaneously recorded traces from the two devices by BIT-FET probes (N). Reprinted by permission from (M, i; and N) Springer Customer Service Centre GmbH: Springer Nature, *Nature Nanotechnology*, Duan et al.,<sup>64</sup> copyright 2011; (M, ii) Fu et al.<sup>77</sup>; and (M, iii) Gao et al.<sup>78</sup> (copyright 2012 American Chemical Society).

Scale bars represent 20 μm (B; M, iii), 150 μm (C), 200 μm (G, left), 5 μm (G, right; J, i), 10 μm (J, ii and iii), 200 nm (M, i), 100 nm (M, ii), and 100 μm (M, iii, inset).

nanoelectronics with planar NW structure, and (3) intracellular electrophysiological studies using 3D nanoprobes with advanced NW structure at the cellular and subcellular levels.

### Semiconductor Nanowire Transistors as Building Blocks for Electrophysiological Signal Recording

The operation schematic of a semiconductor NW FET is shown in Figure 7A. As the fundamental building block for electrophysiological studies, the NW-based FET is a three-terminal structure with source, drain, and gate electrode. Source and drain electrodes are usually metal contacts, which are ohmic-contacted with NW. Current can flow along the semiconductor NW between the source and drain electrodes, which is known as the channel. A naturally grown or deposited oxide layer on the NW can act as the dielectric layer. Similar to a conventional metal-oxide-semiconductor field-effect transistor (MOS-FET), the conductance of the NW can be modulated by the voltage at the gate terminal. Taking doped Si NWs as an example, the electrostatic potential of the NW can be tuned by the gate voltage, which modulates the carrier concentration (holes for p-Si and free electrons for n-Si; Figure 7A, middle) and affects the conductance of the NW. P-type Si devices show a decrease in conductance with increasing gate voltage, and n-type devices display an increase (Figure 7A, bottom). Because a small voltage change in the gate terminal can cause a large variation in the current from source to drain, NW-based FET can significantly magnify the gate signals. In a cellular electrophysiological recording system, the bioelectrical activities, such as action potential, which can simultaneously change the ion concentration and electrical potential both outside and inside the cell, can act as the voltage changes in the gate terminal, and be recorded by the NW-based FET device.

### Extracellular Electrophysiological Study of Cultured Cells, Tissues, and Organs *In Vivo*

Traditionally, electrophysiological recording techniques can be separated into extracellular recording and intracellular recording. For extracellular recording, electrically excitable cells, such as neurons or cardiomyocytes with action potentials or graded potentials, can constantly exchange ions with extracellular fluid.<sup>70</sup> The exchange of ions and propagating waves of ion movement can generate small changes in voltage within a small volume of tissue, which is defined as the local field potential

(LFP), and this LFP can be detected by positioned microelectrode arrays or conventional FET transducers with microscale device dimensions.<sup>71</sup> Compared with those recording methods, NW-based FETs have substantial advantages in achieving nanoscale interfaces between recording transducers and biological systems. Together with signal amplification, NW-based FETs are able to achieve high-quality single-unit extracellular electrophysiological signal recording or large-scale multiplexed recording in complex cellular networks by NW-based FET arrays with high spatio-temporal resolution.

In this field, the Lieber group first applied Si NW FETs for extracellular recording from cultured mammalian neurons in 2006.<sup>72</sup> They grew Si NWs by chemical vapor deposition, fabricated the Si NW FETs on-chip, and passivated the device arrays for cell culture. As shown in Figure 7B, a cortical neuron was interfaced to four NW FETs and axon-crossed NW FET arrays with corresponding signal propagation recorded by NW FETs array, which shows the potential of multiplexed recording with single cellular/subcellular spatial resolution by NW FET arrays. In 2009, Lieber's group reported a flexible method to interface NW FETs with cells for extracellular recording.<sup>73</sup> As shown in Figure 7C, cardiomyocyte cells were cultured on thin polydimethylsiloxane and then contacted with three Si NW FETs. The large signal magnitude indicates that a large seal resistance exists between NW FETs and cardiomyocytes.

Besides on-chip FETs, Lieber's group recently developed a flexible free-standing macroporous nanoelectronic scaffold (nanoES) incorporated with NW FET arrays, which could be used for engineered tissue electrophysiological recording and stimulation.<sup>63,64</sup> As shown in Figure 7D, individually addressable Si NW FETs were incorporated into SU-8, a biocompatible macroporous polymer structure on sacrificial layers by lithography. After etching the sacrificial layer, this free-standing macroporous nanoES was created and can be used for 3D culturing of specific types of cells, including neurons and cardiomyocytes. Figure 7Ei shows the nanoES folded into four layers and culture of cardiac cells. The blue circles show that NW FETs innervate the 3D cell network. The single spike in action potential recorded from 16 sensors from the top layer (Figure 7Eii) and the 3D isochronal map of time latency through the sample (Figure 7Eiii) indicate that the nanoES can achieve real-time 3D mapping and control of *in vitro* cardiomyocytes. This opens new paths for post-surgery heart monitoring and stimulation.

For further development of flexible nanoelectronic platforms and their extension to *in vivo* studies, in 2015, Liu et al.<sup>79</sup> developed a syringe injection strategy for flexible electronics, which includes (1) loading macroporous mesh electronics into a syringe needle, (2) inserting the needle into the brain, (3) injecting the mesh nanoelectronics and withdrawing the needle, and (4) interconnecting input and output. In addition to the syringe injection method, Xie et al.<sup>74</sup> reported another method for *in vivo* study by freezing ultra-flexible probes before the implantation process (Figure 7F). Figure 7G shows the micrograph of frozen ultra-flexible probes marked with NW FET at the end of the supporting arms. After implantation, the *in vivo* LFP can be recorded by NW FET from the barrel cortex area (Figure 7H).

### Intracellular Electrophysiological Study at the Cellular and Subcellular Levels by Advanced Nanowire Structures

Compared with extracellular recording, intracellular recording could provide an entire dynamic range of transmembrane voltage changes, which could push understanding of fundamental biophysical behavior to the molecular level. Moreover, the

subthreshold events from the recorded full action potential are also very important to understand neuronal circuits, although intracellular recording by puncturing the cell plasma membrane is more invasive to cells. In this research field, the patch-clamp technique has been the most widely used for intracellular recording.<sup>71,80</sup> The recording electrode in the micropipette can record intracellular signals when the cell cytosol and the exogenous solution in the pipette mix after the patch-clamp penetrates the cell membrane, but this technique still has some limitations for long-term and multiplexed recording. Recently developed micro- and nanoscale 3D metal electrode arrays with electroporation are able to achieve multiplexed intracellular recording.<sup>81</sup> Nevertheless, self-sealing of electroporation-generated pores and large impedance still limit the quality of the recorded signals, especially in amplitude.

Here, we introduce some recent advances in the development of nanoscale intracellular probes with active NW FET detection components. The small dimensions of these NW transistor probes, together with phospholipid functionalization, make it possible for stable and long-term recording of full-amplitude signals with minimal invasiveness. In 2010, Tian et al.<sup>11</sup> developed 3D kinked NW probes with a point-like FET detector on the tip (Figures 7I and 7Ji), which is the first achievement of full-amplitude intracellular recording by NW FET (Figure 7K). After this pioneering work, Xu et al.<sup>14,75</sup> and Zhao et al.<sup>76</sup> also developed W-shaped NW FET and U-shaped NW FET arrays (Figures 7Jii and 7Jiii), which could be applied for multiplexed recording. In addition, Lieber's group also reported branched intracellular nanotube nano-transistor probes by using a branched SiO<sub>2</sub> nanotube on top of a nanoFET<sup>64,77</sup> and an active nanotube transistor probe<sup>78</sup> for intercellular recording (Figures 7L–7N). The size of the tube could be reduced to sub-10-nm diameter (Figure 7Mii), which opens up unique opportunities for future subcellular electrophysiological studies.

## CONCLUSION

In this review, we focused on merging 1D nanomaterial building blocks with biological systems to generate nano-bio interfaces, which leads to applications in three major fields. (1) In the field of artificial photosynthesis, two general classes of PBSs were discussed. Type I is an integrated nano-bio system that directly transfers electrons from a nanoscale semiconductor light harvester to bacteria; type II is a distributed nano-bio system in which inorganic photocatalysts generate a molecular reducing equivalent such as H<sub>2</sub>, which can be subsequently consumed by bacteria to generate chemical products. We highlighted Si NWs integrated with *Sporomusa ovata* and a CdS-*Moorella thermoacetica* hybrid system as the breakthrough in type I photosynthetic hybrid systems. A hybrid system built from a novel H<sub>2</sub> evolution catalyst, Co-P alloy, and H<sub>2</sub>-oxidizing CO<sub>2</sub> reducing bacteria, *R. eutropha*, which demonstrated energy efficiency of ~10%, was highlighted as the breakthrough in type II photosynthetic hybrid systems. (2) In the field of energy production, the development of MFCs was reviewed. We described the bioelectrochemical mechanisms of MFCs and the feasibility of this bioelectrochemical technology, which converts organic matter to electricity by using biosystems as catalysts. Among various nanoscale structures, NW-based electrodes (such as CNTs, conductive polyaniline NW networks, TiO<sub>2</sub> NWs, and so on) for MFCs show much higher efficiency and sustainability than other structures, such as nanospheres, nanopores, and carbon composites. (3) In the field of nano-bioelectronics, we introduced the basic concept and mechanism of a semiconductor NW-based FET biosensor, followed by a review of extracellular and intracellular electrophysiological studies from cells, tissues, and

organs. We highlighted several unique NW device structures, such as 3D kinked NW probes with a point-like FET detector on the tip, branched intracellular nanotube nano-transistor probes using a branched SiO<sub>2</sub> nanotube on top of a nanoFET, and an active nanotube transistor probe for intercellular recordings.

On the basis of the development of inorganic-biological hybrid systems, we would like to emphasize some future directions that could lead to significant progress in the nano-bio interdisciplinary field. First, the current bottlenecks of PBSs are volumetric productivity and the production rate. The volumetric productivity is limited by the bulky nature of microorganisms. A high production rate would cause severe oxidative conditions, which would damage the biological system. To address these issues, optimizing the nano-bio interface using larger surface area electrodes and synthesizing high-density nanoscale inorganic materials from the bacteria might be considered. Second, MFCs are attractive as green energy, but have low energy and power densities. Design of highly conductive NW networks and further improvement of the contact between the bacteria and NW electrodes would increase the electron-transfer efficiency between biological system and inorganic electrodes. Third, NW transistor devices have been successfully demonstrated as a unique tool for high spatiotemporal resolution detection of biological signals at cellular and even subcellular level. Combining the strengths of the bottom-up synthetic approach and top-down nanofabrication techniques to assemble NW FET devices on a large scale and realize multiplexed cellular/subcellular electrical signal recordings of neurons could open up new perspectives on the complex circuitry and computations in the brain, particularly for *in vivo* studies.

## ACKNOWLEDGMENTS

This work was supported by the National Key Research and Development Program of China (2016YFA0202603), the National Basic Research Program of China (2013CB934103), the Program of Introducing Talents of Discipline to Universities (B17034), the National Natural Science Foundation of China (51521001), the National Natural Science Fund for Distinguished Young Scholars (51425204), the Yellow Crane Talent (Science & Technology) Program of Wuhan City, and the Fundamental Research Funds for the Central Universities (WUT: 2016III001 and 2017III009). The authors thank Prof. C.M. Lieber at Harvard University and Prof. P. Yang at the University of California, Berkeley, for their strong support.

## AUTHOR CONTRIBUTIONS

L.M. proposed the topic of the review and supervised the writing of the manuscript. L.X., Y.Z., K.A.O., Z.Z., Q.L., Z.L., and Z.W. investigated the literature and wrote the original manuscript. All authors discussed and revised the manuscript. L.X and Y.Z. contributed equally to this work.

## REFERENCES AND NOTES

- Blankenship, R.E., Tiede, D.M., Barber, J., Brudvig, G.W., Fleming, G., Ghirardi, M., Gunner, M.R., Junge, W., Kramer, D.M., Melis, A., et al. (2011). Comparing photosynthetic and photovoltaic efficiencies and recognizing the potential for improvement. *Science* 332, 805–809.
- Lieber, C.M. (2011). Semiconductor nanowires: a platform for nanoscience and nanotechnology. *MRS Bull.* 36, 1052–1063.
- Gudiksen, M.S., and Lieber, C.M. (2000). Diameter-selective synthesis of semiconductor nanowires. *J. Am. Chem. Soc.* 122, 8801–8802.
- Shi, Y., Hu, Q., Araki, H., Suzuki, H., Gao, H., Yang, W., and Noda, T. (2005). Long Si nanowires with millimeter-scale length by modified thermal evaporation from Si powder. *Appl. Phys. A.* 80, 1733–1736.
- Jeong, H.E., Kim, I., Karam, P., Choi, H.J., and Yang, P. (2013). Bacterial recognition of silicon nanowire arrays. *Nano Lett.* 13, 2864–2869.
- Cui, Y., Wei, Q., Park, H., and Lieber, C.M. (2001). Nanowire nanosensors for highly sensitive and selective detection of

- biological and chemical species. *Science* 293, 1289–1292.
7. Patolsky, F., Zheng, G., Hayden, O., Lakadamyali, M., Zhuang, X., and Lieber, C.M. (2004). Electrical detection of single viruses. *Proc. Natl. Acad. Sci. USA* 101, 14017–14022.
  8. Patolsky, F., Zheng, G., and Lieber, C.M. (2006). Nanowire-based biosensors. *Anal. Chem.* 78, 4260–4269.
  9. Zhang, F., Jiang, Y., Liu, X., Meng, J., Zhang, P., Liu, H., Yang, G., Li, G., Jiang, L., and Wan, L.J. (2016). Hierarchical nanowire arrays as three-dimensional fractal nano-biointerfaces for high efficient capture of cancer cells. *Nano Lett.* 16, 766–772.
  10. Hai, A., Shappir, J., and Spira, M.E. (2010). In-cell recordings by extracellular microelectrodes. *Nat. Methods* 7, 200–202.
  11. Tian, B., Cohen-Karni, T., Quan, Q., Duan, X., Xie, P., and Lieber, C.M. (2010). Three-dimensional, flexible nanoscale field effect transistors as localized bioprobes. *Science* 329, 830–834.
  12. Zimmerman, J.F., Murray, G.F., Wang, Y., Jumper, J.M., Ii, J.R.A., and Tian, B. (2015). Free-standing kinked silicon nanowires for probing inter- and intracellular force dynamics. *Nano Lett.* 15, 5492–5498.
  13. Kong, B., Tang, J., Wu, Z., Selomulya, C., Wang, H., Wei, J., Wang, Y., Zheng, G., and Zhao, D. (2014). Bio-inspired porous antenna-like nanocube/nanowire heterostructure as ultra-sensitive cellular interfaces. *NPG. Asia. Mater.* 6, e117.
  14. Xu, L., Jiang, Z., Quan, Q., Mai, L., Zhang, Q., and Lieber, C.M. (2013). Design and synthesis of diverse functional kinked nanowire structures for nanoelectronic bioprobes. *Nano Lett.* 13, 746–751.
  15. Sakimoto, K.K., Kornienko, N., and Yang, P.D. (2017). Cyborgian material design for solar fuel production: the emerging photosynthetic biohybrid systems. *Acc. Chem. Res.* 50, 476–481.
  16. Nevin, K.P., Woodard, T.L., Franks, A.E., Summers, Z.M., and Lovley, D.R. (2010). Microbial electrosynthesis: feeding microbes electricity to convert carbon dioxide and water to multicarbon extracellular organic compounds. *mBio* 1, 4.
  17. Rabaey, K., and Rozendal, R.A. (2010). Microbial electrosynthesis - revisiting the electrical route for microbial production. *Nat. Rev. Microbiol.* 8, 706–716.
  18. Sakimoto, K.K., Liu, C., Lim, J., and Yang, P.D. (2014). Salt-induced self-assembly of bacteria on nanowire arrays. *Nano Lett.* 14, 5471–5476.
  19. Nichols, E.M., Gallagher, J.J., Liu, C., Su, Y.D., Resasco, J., Yu, Y., Sun, Y.J., Yang, P.D., Chang, M.C.Y., and Chang, C.J. (2015). Hybrid bioinorganic approach to solar-to-chemical conversion. *Proc. Natl. Acad. Sci. USA* 112, 11461–11466.
  20. Liu, C., Gallagher, J.J., Sakimoto, K.K., Nichols, E.M., Chang, C.J., Chang, M.C.Y., and Yang, P.D. (2015). Nanowire-bacteria hybrids for unassisted solar carbon dioxide fixation to value-added chemicals. *Nano Lett.* 15, 3634–3639.
  21. Liu, C., Tang, J.Y., Chen, H.M., Liu, B., and Yang, P.D. (2013). A fully integrated nanosystem of semiconductor nanowires for direct solar water splitting. *Nano Lett.* 13, 2989–2992.
  22. Sakimoto, K.K., Wong, A.B., and Yang, P.D. (2016). Self-photosensitization of nonphotosynthetic bacteria for solar-to-chemical production. *Science* 351, 74–77.
  23. Deutzmans, J.S., Sahin, M., and Spormann, A.M. (2015). Extracellular enzymes facilitate electron uptake in biocorrosion and bioelectrosynthesis. *mBio* 6, 8.
  24. Kornienko, N., Sakimoto, K.K., Herlihy, D.M., Nguyen, S.C., Alivisatos, A.P., Harris, C.B., Schwartzberg, A., and Yang, P.D. (2016). Spectroscopic elucidation of energy transfer in hybrid inorganic-biological organisms for solar-to-chemical production. *Proc. Natl. Acad. Sci. USA* 113, 11750–11755.
  25. Sakimoto, K.K., Zhang, S.J., and Yang, P.D. (2016). Cysteine-cystine photoregeneration for oxygenic photosynthesis of acetic acid from CO<sub>2</sub> by a tandem inorganic-biological hybrid system. *Nano Lett.* 16, 5883–5887.
  26. Balzani, V., and Armaroli, N. (2010). Energy for a Sustainable World: From the Oil Age to a Sun-powered Future (John Wiley).
  27. Torella, J.P., Gagliardi, C.J., Chen, J.S., Bediako, D.K., Colon, B., Way, J.C., Silver, P.A., and Nocera, D.G. (2015). Efficient solar-to-fuels production from a hybrid microbial-water-splitting catalyst system. *Proc. Natl. Acad. Sci. USA* 112, 2337–2342.
  28. Liu, C., Colon, B.C., Ziesack, M., Silver, P.A., and Nocera, D.G. (2016). Water splitting-biosynthetic system with CO<sub>2</sub> reduction efficiencies exceeding photosynthesis. *Science* 352, 1210–1213.
  29. Bullen, R.A., Arnot, T.C., Lakeman, J.B., and Walsh, F.C. (2006). Biofuel cells and their development. *Biosens. Bioelectron.* 21, 2045–2045.
  30. Babu, M.L., Subhash, G.V., Sarma, P.N., and Mohan, S.V. (2013). Bio-electrolytic conversion of acidogenic effluents to biohydrogen: an integration strategy for higher substrate conversion and product recovery. *Bioresour. Technol.* 133, 322–331.
  31. Xing, D.F., Yi, Z., Cheng, S.A., Regan, J.M., and Logan, B.E. (2008). Electricity generation by *Rhodopseudomonas palustris* DX-1. *Environ. Sci. Technol.* 42, 4146–4151.
  32. Liang, B., Cheng, H.Y., Kong, D.Y., Gao, S.H., Sun, F., Cui, D., Kong, F.Y., Zhou, A.J., Liu, W.Z., and Ren, N.Q. (2013). Accelerated reduction of chlorinated nitroaromatic antibiotic chloramphenicol by biocathode. *Environ. Sci. Technol.* 47, 5353–5361.
  33. Lovley, D.R. (2008). The microbe electric: conversion of organic matter to electricity. *Curr. Opin. Biotechnol.* 19, 564–571.
  34. Jiang, X., Hu, J., Fitzgerald, L.A., Biffinger, J.C., Xie, P., Ringelsen, B.R., and Lieber, C.M. (2010). Probing electron transfer mechanisms in *Shewanella oneidensis* MR-1 using a nanoelectrode platform and single-cell imaging. *Proc. Natl. Acad. Sci. USA* 107, 16806–16810.
  35. Jiang, X., Hu, J., Petersen, E.R., Fitzgerald, L.A., Jackan, C.S., Lieber, A.M., Ringelsen, B.R., Lieber, C.M., and Biffinger, J.C. (2013). Probing single- to multi-cell level charge transport in *Geobacter sulfurreducens* DL-1. *Nat. Commun.* 4, 2751.
  36. He, Z., Minteer, S.D., and Angenent, L.T. (2005). Electricity generation from artificial wastewater using an upflow microbial fuel cell. *Environ. Sci. Technol.* 39, 5262–5267.
  37. Xie, X., Ye, M., Hu, L.B., Liu, N., McDonough, J.R., Wei, C., Alshareef, H.N., Criddle, C.S., and Cui, Y. (2012). Carbon nanotube-coated macroporous sponge for microbial fuel cell electrodes. *Energy Environ. Sci.* 5, 5265–5270.
  38. Saito, T., Mehanna, M., Xin, W., Cusick, R.D., Feng, Y.J., Hickner, M.A., Logan, B.E., Pandey, A., Lee, D.J., and Logan, B.E. (2011). Effect of nitrogen addition on the performance of microbial fuel cell anodes. *Bioresour. Technol.* 102, 395–398.
  39. Kalathil, S., Van, N.H., Shim, J.J., Khan, M.M., Lee, J., and Cho, M.H. (2013). Enhanced performance of a microbial fuel cell using CNT/MnO<sub>2</sub> nanocomposite as a bioanode material. *J. Nanosci. Nanotechnol.* 13, 7712–7716.
  40. Zhao, Y., Watanabe, K., Nakamura, R., Mori, S., Liu, H., Ishii, K., and Hashimoto, K. (2010). Three-dimensional conductive nanowire networks for maximizing anode performance in microbial fuel cells. *Chemistry* 16, 4982–4985.
  41. Zhao, Y., Nakanishi, S., Watanabe, K., and Hashimoto, K. (2011). Hydroxylated and aminated polyaniline nanowire networks for improving anode performance in microbial fuel cells. *J. Biosci. Bioeng.* 112, 63–66.
  42. Jia, X.Q., He, Z.H., Zhang, X., and Tian, X.J. (2016). Carbon paper electrode modified with TiO<sub>2</sub> nanowires enhancement bioelectricity generation in microbial fuel cell. *Synth. Met.* 215, 170–175.
  43. Zhang, A.Q., and Lieber, C.M. (2015). Nano-bioelectronics. *Chem. Rev.* 116, 215–257.
  44. Kwak, M., Han, L., Chen, J.J., and Fan, R. (2015). Interfacing inorganic nanowire arrays and living cells for cellular function analysis. *Small* 11, 5600–5610.
  45. Roszek, B., De Jong, W., and Geertsma, R. (2005). Nanotechnology in medical applications: state-of-the-art in materials and devices. RIVM Report 265001001. <https://www.rivm.nl/dsresource?objectid=7a58ee1c-db59-4b87-8b97-0ba615d5566a&type=org&disposition=inline>.
  46. Peng, F., Su, Y.Y., Zhong, Y.L., Fan, C.H., Lee, S.T., and He, Y. (2014). Silicon nanomaterials platform for bioimaging, biosensing, and cancer therapy. *Acc. Chem. Res.* 47, 612–623.
  47. Duan, X.J., and Lieber, C.M. (2015). Nanoscience and the nano-bioelectronics frontier. *Nano Res.* 8, 1–22.
  48. Patolsky, F., and Lieber, C.M. (2005). Nanowire nanosensors. *Mater. Today* 8, 20–28.

49. Patolsky, F., Timko, B.P., Zheng, G., and Lieber, C.M. (2007). Nanowire-based nanoelectronic devices in the life sciences. *MRS Bull.* 32, 142–149.
50. Chen, K.I., Li, B.R., and Chen, Y.T. (2011). Silicon nanowire field-effect transistor-based biosensors for biomedical diagnosis and cellular recording investigation. *Nano Today* 6, 131–154.
51. Wang, S.T., Liu, K., Liu, J., Yu, Z.T.F., Xu, X.W., Zhao, L.B., Lee, T., Lee, E.K., Reiss, J., and Lee, Y.K. (2011). Highly efficient capture of circulating tumor cells by using nanostructured silicon substrates with integrated chaotic micromixers. *Angew. Chem. Int. Ed.* 50, 3084–3088.
52. Kim, S.T., Kim, D.J., Kim, T.J., Seo, D.W., Kim, T.H., Lee, S.Y., Kim, K., Lee, K.M., and Lee, S.K. (2010). Novel streptavidin-functionalized silicon nanowire arrays for CD4+ T lymphocyte separation. *Nano Lett.* 10, 2877–2883.
53. Zhao, L.B., Lu, Y.T., Li, F.Q., Wu, K., Hou, S., Yu, J., Shen, Q.L., Wu, D.X., Song, M., and Ouyang, W.H. (2013). High-purity prostate circulating tumor cell Isolation by a polymer nanofiber-embedded microchip for whole exome sequencing. *Adv. Mater.* 25, 2897–2902.
54. Prinz, C., Hällström, W., Mårtensson, T., Samuelson, L., Montelius, L., and Kanje, M. (2008). Axonal guidance on patterned free-standing nanowire surfaces. *Nanotechnol.* 19, 345101.
55. Johansson, F., Jonsson, M., Alm, K., and Kanje, M. (2010). Cell guidance by magnetic nanowires. *Exp. Cell Res.* 316, 688–694.
56. Hällström, W., Lexholm, M., Suyatin, D.B., Hammarin, G., Hessman, D., Samuelson, L., Montelius, L., Kanje, M., and Prinz, C.N. (2010). Fifteen-picnewton force detection from neural growth cones using nanowire arrays. *Nano Lett.* 10, 782–787.
57. Li, Z., Song, J.H., Mantini, G., Lu, M.Y., Fang, H., Falconi, C., Chen, L.J., and Wang, Z.L. (2009). Quantifying the traction force of a single cell by aligned silicon nanowire array. *Nano Lett.* 9, 3575–3580.
58. Xie, X., Xu, A.M., Angle, M.R., Tayebi, N., Verma, P., and Melosh, N.A. (2013). Mechanical model of vertical nanowire cell penetration. *Nano Lett.* 13, 6002–6008.
59. Kim, W., Ng, J.K., Kunitake, M.E., Conklin, B.R., and Yang, P. (2007). Interfacing silicon nanowires with mammalian cells. *J. Am. Chem. Soc.* 129, 7228–7229.
60. Wang, L.L., Shalek, A.K., Lawrence, M., Ding, R., Gaublomme, J.T., Pochet, N., Stojanov, P., Sougnez, C., Shukla, S.A., and Stevenson, K.E. (2014). Somatic mutation as a mechanism of Wnt/B-catenin pathway activation in CLL. *Blood* 124, 1089–1098.
61. Shalek, A.K., Robinson, J.T., Karp, E.S., Lee, J.S., Ahn, D.R., Yoon, M.H., Sutton, A., Jorgoll, M., Gertner, R.S., and Gujral, T.S. (2010). Vertical silicon nanowires as a universal platform for delivering biomolecules into living cells. *Proc. Natl. Acad. Sci. USA* 107, 1870–1875.
62. Vandersarl, J.J., Xu, A.M., and Melosh, N.A. (2011). Nanostraws for direct fluidic intracellular access. *Nano Lett.* 12, 3881–3886.
63. Dai, X.C., Zhou, W., Gao, T., Liu, J., and Lieber, C.M. (2016). Three-dimensional mapping and regulation of action potential propagation in nanoelectronics-innervated tissues. *Nat. Nanotechnol.* 11, 776–782.
64. Duan, X.J., Gao, R.X., Xie, P., Cohen Karni, T., Qing, Q., Choe, H.S., Tian, B., Jiang, X.C., and Lieber, C.M. (2012). Intracellular recordings of action potentials by an extracellular nanoscale field-effect transistor. *Nat. Nanotechnol.* 7, 174–179.
65. Tian, B., Liu, J., Dvir, T., Jin, L., Tsui, J.H., Qing, Q., Suo, Z., Langer, R., Kohane, D.S., and Lieber, C.M. (2012). Macroporous nanowire nanoelectronic scaffolds for synthetic tissues. *Nat. Mater.* 11, 986–994.
66. Lin, Z.C., Xie, C., Osakada, Y., Cui, Y., and Cui, B. (2014). Iridium oxide nanotube electrodes for sensitive and prolonged intracellular measurement of action potentials. *Nat. Commun.* 5, 3206.
67. Yan, R.X., Park, J.H., Choi, Y., Heo, C.J., Yang, S.M., Lee, L.P., and Yang, P.D. (2012). Nanowire-based single-cell endoscopy. *Nat. Nanotechnol.* 7, 191–196.
68. Robinson, J.T., Jorgoll, M., Shalek, A.K., Yoon, M.H., Gertner, R.S., and Park, H. (2012). Vertical nanowire electrode arrays as a scalable platform for intracellular interfacing to neuronal circuits. *Nat. Nanotechnol.* 7, 180–184.
69. Narahashi, T. (2003). Principles of electrophysiology: an overview. *Curr. Protoc. Toxicol. Chapter 11. Unit 11.10.*
70. Hille, B. (2001). *Ion Channels of Excitable Membranes* (Sinauer).
71. Wickenden, A.D. (2014). Overview of electrophysiological techniques. *Curr. Protoc. Pharmacol.* 64, 11.1.1–11.1.17.
72. Patolsky, F., Timko, B.P., Yu, G., Fang, Y., Greytak, A.B., Zheng, G., and Lieber, C.M. (2006). Detection, stimulation, and inhibition of neuronal signals with high-density nanowire transistor arrays. *Science* 313, 1100–1104.
73. Cohen Karni, T., Timko, B.P., Weiss, L.E., and Lieber, C.M. (2009). Flexible electrical recording from cells using nanowire transistor arrays. *Proc. Natl. Acad. Sci. USA* 106, 7309–7313.
74. Xie, C., Liu, J., Fu, T.M., Dai, X.C., Zhou, W., and Lieber, C.M. (2015). Three-dimensional macroporous nanoelectronic networks as minimally invasive brain probes. *Nat. Mater.* 14, 1286–1292.
75. Xu, L., Jiang, Z., Mai, L.Q., and Qing, Q. (2014). Multiplexed free-standing nanowire transistor bioprobe for intracellular recording: A general fabrication strategy. *Nano Lett.* 14, 3602–3607.
76. Zhao, Y.L., Yao, J., Xu, L., Mankin, M.N., Zhu, Y.B., Wu, H., Mai, L.Q., Zhang, Q.J., and Lieber, C.M. (2016). Shape-controlled deterministic assembly of nanowires. *Nano Lett.* 16, 2644–2650.
77. Fu, T.M., Duan, X., Jiang, Z., Dai, X.C., Xie, P., Cheng, Z.G., and Lieber, C.M. (2014). Sub-10-nm intracellular bioelectronic probes from nanowire–nanotube heterostructures. *Proc. Natl. Acad. Sci. USA* 111, 1259–1264.
78. Gao, R.X., Strehle, S., Tian, B., Cohen Karni, T., Xie, P., Duan, X.J., Qing, Q., and Lieber, C.M. (2012). Outside looking in: Nanotube transistor intracellular sensors. *Nano Lett.* 12, 3329–3333.
79. Liu, J., Fu, T.M., Cheng, Z.G., Hong, G.S., Zhou, T., Jin, L.H., Duvvuri, M., Jiang, Z., Kruskal, P., and Xie, C. (2015). Syringe-injectable electronics. *Nat. Nanotechnol.* 10, 629–636.
80. Hamill, O.P., Marty, A., Neher, E., Sakmann, B., and Sigworth, F. (1981). Improved patch-clamp techniques for high-resolution current recording from cells and cell-free membrane patches. *Pflügers Arch. Eur. J. Physiol.* 391, 85–100.
81. Spira, M.E., and Hai, A. (2013). Multi-electrode array technologies for neuroscience and cardiology. *Nat. Nanotechnol.* 8, 83–94.